Journal of Medicinal Chemistry

ARTICLE

pubs.acs.org/jmc

Curcumin Recognizes a Unique Binding Site of Tubulin

Soumyananda Chakraborti,[†] Lalita Das,[†] Neha Kapoor,[‡] Amlan Das,[§] Vishnu Dwivedi,[‡] Asim Poddar,[†] Gopal Chakraborti,[§] Mark Janik,[∥] Gautam Basu,[⊥] Dulal Panda,[#] Pinak Chakrabarti,[†] Avadhesha Surolia,[‡,*] and Bhabatarak Bhattacharyya[*,†]

[†]Department of Biochemistry, Bose Institute, Centenary Campus, P-1/12 CIT Scheme VIIM, Kolkata 700054, India

[‡]Centre for Molecular Medicine, National Institute of Immunology, New Delhi 110012, India

[§]Dr BC Guha Centre for Genetic Engineering & Biotechnology, University of Calcutta, Kolkata 700019, India

[∥]Department of Chemistry, SUNY Fredonia, Fredonia, New York 14063, United States

[⊥]Department of Biophysics, Bose Institute, P-1/12 CIT Scheme VIIM, Kolkata 700054, India

[#]Department of Bioscience and Bioengineering, Indian Institute of Technology Bombay, Mumbai 400076, India

Supporting Information

ABSTRACT: Although curcumin is known for its anticarcinogenic properties, the exact mechanism of its action or the identity of the target receptor is not completely understood. Studies on a series of curcumin analogues, synthesized to investigate their tubulin binding affinities and tubulin self-assembly inhibition, showed that: (i) curcumin acts as a bifunctional ligand, (ii) analogues with substitution at the diketone and acetylation of the terminal phenolic groups of curcumin are less effective, (iii) a benzylidiene derivative, compound 7, is more effective than curcumin in inhibiting tubulin self-assembly. Cell-based studies also showed compound 7 to be more effective than curcumin. Using fluorescence spectroscopy we show that curcumin binds tubulin 32 Å away from the colchicine-binding site. Docking studies also suggests that the curcumin-binding site to be close to the vinblastine-binding site. Structure−activity studies suggest that the tridented nature of compound 7 is responsible for its higher affinity for tubulin compared to curcumin.

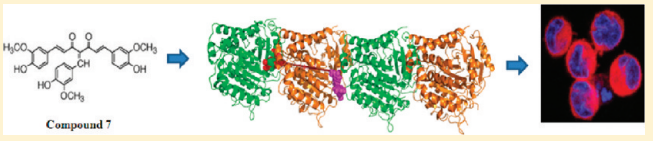

INTRODUCTION

Tubulin is an essential eukaryotic protein that plays critical roles in cell division and is an established target of anticancer drug development. This interest in tubulin as a chemotherapeutic target has initiated the investigation of the molecular nature of tubulin−drug binding sites. Because a significant number of anticancer drugs are antimicrotubule agents, new antimitotic natural products are continuously being discovered and considered for cancer chemotherapy. Although these drugs are structurally diverse,[1] often they employ a common mechanism of action and, surprisingly, nature has repeatedly validated tubulin as a drug target.[2] Both taxol and vinblastine show unique clinical utilities. However, in both the cases resistance is exhibited by cancer cells at the later stages of treatment.[3,4] Furthermore, both drugs have significant toxicity and other side effects on human physiology.[5] Interestingly, there is compelling evidence from epidemiological and other experimental studies that highlight the importance of many dietary agents such as soyaisoflavone, resveratrol, genistein, napthoquinone plumbagin, and curcumin in reducing the risk of cancer and inhibition of the development and spread of tumors in experimental animals.[6,7] The advantage of using such compounds for cancer treatment is their relatively nontoxic nature and availability in an ingestive form.[8]

Curcumin, a phytochemical known for its medicinal properties, is currently in phase II clinical trials in patients with advanced pancreatic cancer.[9] Originally isolated from the rhizomes of *Curcuma longa*, curcumin is characterized by a wide range of medicinal properties like antibacterial, antifungal, antiviral, antioxidative, anti-inflammatory, and antiproliferative.[10] In addition to its broad range of bioactivities, curcumin is also known for its strong cancer preventive activity against a wide range of tumor cells[11] and prevention of tumor initiation, promotion, metastasis, and angiogenesis in experimental animal systems.[10,12] An important mechanism by which curcumin inhibits tumorigenesis is by suppressing oncogenic cell proliferation by inducing apoptosis and arresting cell cycle progression.[13] Recently, curcumin has been shown to arrest cancer cells in the G2-M phase mainly by altering the expression of many crucial genes responsible for the G2-M transition.[14] Curcumin is also known to cause mitochondrial damage and activate both caspase-dependent and caspase-independent apoptosis in various cancer cell lines.[15,16] Through rigorous screening processes and preclinical studies, curcumin has emerged as a potential new chemopreventive agent due to its wide range of anticancer activity and, especially, the absence of any associated toxicity even at high concentrations.[10,17] As a multitarget molecule, a long list of targets/receptors for curcumin has been reported.[10] For example, it was suggested that

Received: April 5, 2011
Published: August 10, 2011

Table 1. Spectral Properties, Physical Characteristics, and Half Maximum Polymerization Inhibition Value of Different Curcumin Analogues

Compd	Structure	Chemical name	Absorbance maxima (nm)	Half maximum polymerization inhibition value (μM)
1	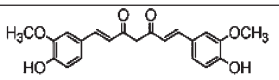	Curcumin	427	20
2	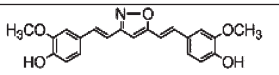	Isoxazole analog of curcumin	333	26
3	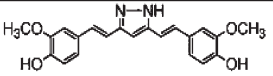	Curcumin pyrazole	327	23
4	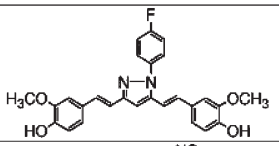	N-(4-Fluorophenylpyrazole) curcumin	332	34
5	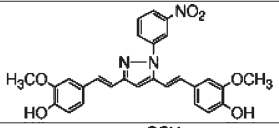	N-(3-Nitrophenylpyrazole) curcumin	334	36
6	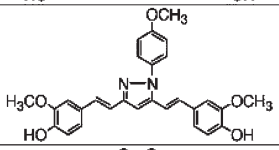	N-(4-Methoxyphenylpyrazole) curcumin	332	38
7	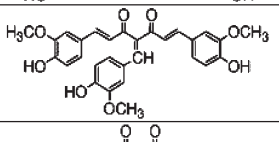	4-(4-Hydroxy-3-methoxy benzylidene) curcumin	370	16
8	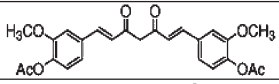	Di-O-acetylcurcumin	413	60
9	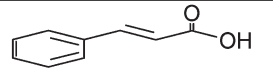	3-phenylprop-2-enoic acid	273 (MeOH)	----
10	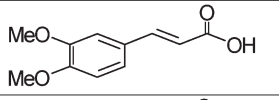	3-(3,4-dimethoxyphenyl) prop-2-enoic acid	284 (MeOH)	---
11	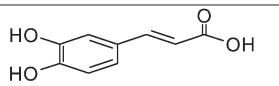	3-(3,4-dihydroxyphenyl) prop-2-enoic acid	320 (MeOH)	---
12	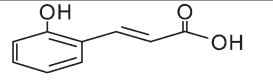	3-(2-hydroxyphenyl) prop-2-enoic acid	321 (MeOH)	---
13	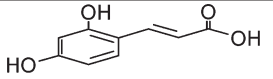	3-(2,4-dihydroxyphenyl) prop-2-enoic acid	319 (MeOH)	---

curcumin directly inhibits IKK and the 26S proteosome to block NF-$\kappa\beta$ activation.[18] This conclusion was drawn on the basis of cell-based studies with no report of in vitro purification of the target or the receptor.[18]

Recently, Gupta et al. have shown that curcumin inhibits HeLa and MCF-7 cell proliferation, disrupts microtubule assembly in vitro, reduces GTPase activity, and partially inhibits colchicine's binding activity,[19] strongly suggesting that curcumin interacts with dimeric tubulin or microtubules. More recently, Banerjee et al. from the same laboratory reported that curcumin suppresses the dynamic instability of microtubules in MCF-7 cells.[20] The microtubule network in eukaryotic cells is an essential component of the cytoskeleton and plays a pivotal role in a variety of cell signaling events.[21] A large number of antimitotic

dx.doi.org/10.1021/jm2004046 |J. Med. Chem. 2011, 54, 6183–6196

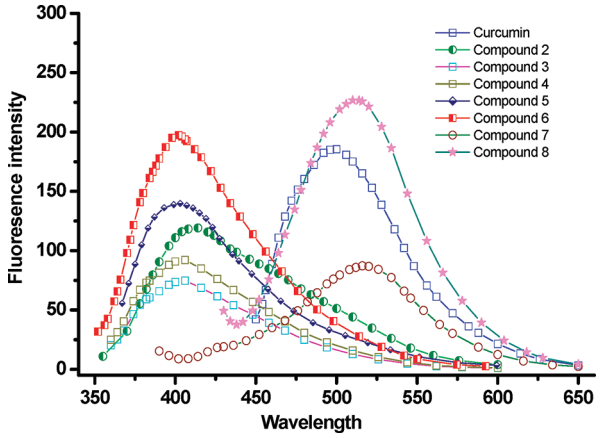

Figure 1. Fluorescence spectra of different curcumin analogues in presence of tubulin. The complexes were excited at their characteristic wavelength maxima, which were 330 nm for compounds **2**−**6**, 427 nm for curcumin and compound **8**, and 370 nm for compound **7**.

drugs bind tubulin or microtubules at one of the three characterized tubulin ligand sites: taxol, colchicine, and vinca-binding sites.[22] Each site can accommodate compounds with very different structures.[23] Among the three binding sites, taxol-site binding drugs possess a unique ability to induce microtubule assembly. Therefore, as an inhibitor of microtubule assembly, curcumin cannot be a likely candidate for the taxol-binding site of tubulin. Rather, curcumin probably targets one of the remaining two sites or a unique new site. Gupta et al. also reported that colchicine and podophyllotoxin partly inhibited the binding of curcumin to tubulin, while vinblastine had no effect on the curcumin−tubulin interaction.[19] Curcumin is a symmetric bidented ligand containing two α,β-unsaturated-diketone moieties flanked by 4-hydroxy-3-methoxyphenyl groups (Table 1). These diketones at the middle and the hydroxyl group at the two terminal phenyl rings are responsible for the instability of curcumin in aqueous solution.[24] To probe the effect of perturbing the structure and chemical nature of curcumin on curcumin-binding to tubulin, we synthesized a number of curcumin analogues (compounds **2**−**13**; Table 1) and examined their binding with purified tubulin. These included curcumin and its analogues with an isoxazole ring compound **2**, a pyrazole ring compound **3**, and substituted pyrazole ring, compounds **4**−**6**, in place of the dicarbonyl moiety, and a 4-hydroxy-3-methoxyphenyl in between the dicarbonyl moiety compound **7**. We also synthesized an analogue where the phenolic groups in the terminal rings are acetylated compound **8**, and a number of single ring-curcumin analogues, compounds **9**−**13**. Screening of the synthesized compounds, by determining their binding affinity for tubulin, their capacity to inhibit tubulin self-assembly, and cell-based study using fluorescence microscopy, has been performed. The thermodynamic parameters associated with curcumin and compound **7** binding to tubulin have been determined using isothermal titration calorimetry (ITC) and different fluorescence techniques. Fluorescence resonance energy transfer (FRET) was observed between colchicine and curcumin when colchicine−tubulin complex was titrated with curcumin. Analysis of FRET results showed that curcumin binds tubulin at some unique position located about 32 Å away from the colchicine-binding site. A detailed comparison of interactions of curcumin and the curcumin analogues with tubulin allowed us

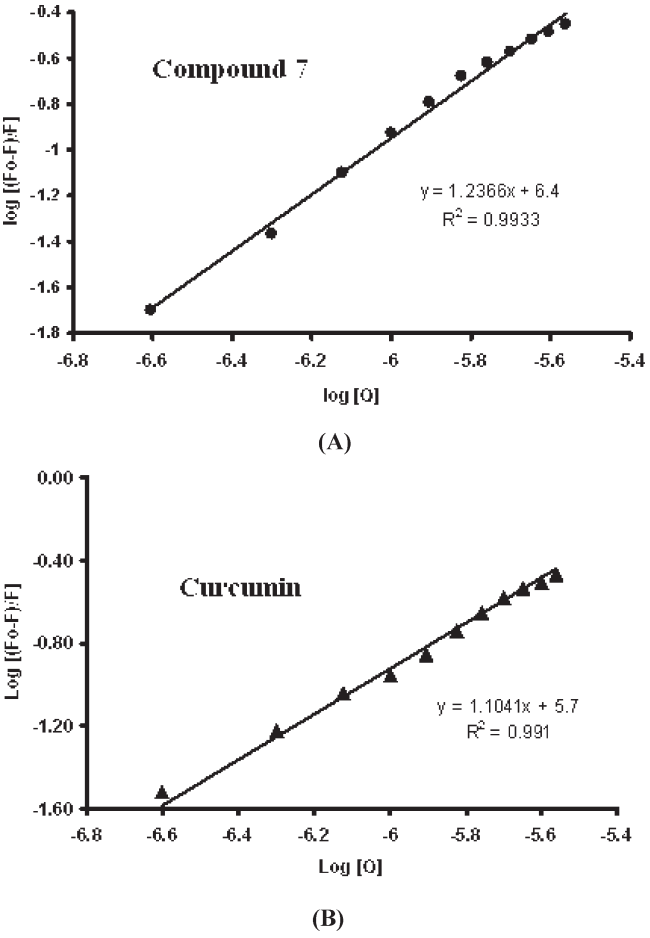

Figure 2. Plot of $\log[(F_o - F)/F]$ against log [Q] derived from the quenching of tubulin by compound **7** and curcumin respectively (Quencher in the plot). The equation of the fitted line is also shown.

to pinpoint the structure−function relationship of the curcumin−tubulin interaction. In addition, using molecular modeling and FRET, we attempt to understand the relationship between the curcumin-binding site of tubulin and two other canonical drug-binding sites on tubulin−colchicine and vinblastine.

RESULTS

Binding of Curcumin Analogues to Tubulin Promote Drug Fluorescence. One of our main objectives was to synthesize various analogues of curcumin that would exhibit a higher affinity toward tubulin, thus enhancing the inhibitory activity of curcumin against cancer cell proliferation. Toward this goal, three types of curcuminoids[25] were synthesized: (i) isoxazole derivative of curcumin, compound **2**, (ii) pyrazole derivatives of curcumin, compounds **3**−**6**, and (iii) a benzylidiene derivative of curcumin, compound **7**. Apart from these, we also synthesized a di-*O*-acetyl derivative of curcumin, compound **8**. Binding of curcumin and its derivatives with purified tubulin was studied using fluorescence. Fluorescence spectra (Figure 1) of tubulin-bound curcumin analogues showed that curcumin and its two analogues, compounds **7** and **8**, exhibit fluorescence emission at a much higher wavelength compared to other analogues. These three compounds possess an extended π−electron delocalization system and exhibit characteristic emission maxima near

dx.doi.org/10.1021/jm2004046 |*J. Med. Chem.* 2011, 54, 6183–6196

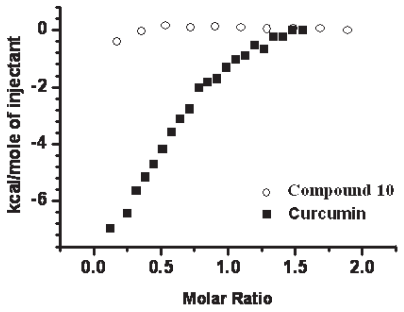

Figure 3. Calorimetric titration of curcumin and its half analogue compound **10** with tubulin. ITC data obtained from 25 injections of 10 μL aliquots of curcumin into 0.030 mM tubulin in 50 mM PIPES buffer (pH 7.0). The heat evolved per mol of curcumin against the molar ratio (ligand:tubulin) for each injection has been plotted.

Table 2. Thermodynamics of Tubulin−Curcumin Binding at 30 °C

parameter	value (standard deviation)
N (drug:protein stoichiometry)	0.62 ± 0.01
K_a (binding constant, M^{-1})	4.5 ± 0.4 × 10^5
ΔH (binding enthalpy, kcal/mol)	−6.62 ± 0.18
ΔS_{tot} (entropy change, cal/mol.K)	4
ΔS_{solv} (cal K^{-1} mol^{-1})	132.8
ΔS_{conf} (cal K^{-1} mol^{-1})	−120.8
$\Delta S_{r/t}$ (cal K^{-1} mol^{-1})	−8
ΔG (Free energy change, kcal/mol)	−7.88

500 nm when bound to tubulin. The remaining curcumin analogues exhibit characteristic fluorescence maxima near 400 nm. These are basically pyrazole, isaoxazole, and *N*-(substituted) phenylpyrazole curcumin (Table 1). The substitution in the diketone group in these molecules produces structural alterations that hinder extended conjugation, therefore resulting in a blue-shift in the absorption maxima.

Determination of Binding Constant and Thermodynamics. Affinity constants of compound 7 and curcumin toward purified tubulin were determined from fluorescence-monitored drug−tubulin titration using a modified Stern−Volmer equation (Figure 2). Compound 7 was characterized by a binding affinity (K_a = 2.5 × 10^6 M^{-1}) toward tubulin that was five times higher compared to curcumin (K_a = 5.01 × 10^5 M^{-1}). To decipher the nature of the interaction of curcumin with tubulin, curcumin−tubulin binding was further studied using ITC. Figure 3 shows the fitted titration data of tubulin with curcumin in PEM buffer at 30 °C. The associated thermodynamic parameters (ΔG, ΔH, and ΔS) are presented in Table 2. The addition of curcumin resulted in an exothermic ligand binding event with an association constant of 4.5 × 10^5 M^{-1}, compatible to the value obtained from the fluorescence data. We could not measure the binding constant between compound 7 and tubulin using calorimetery due to the poor solubility of compound 7 in aqueous solution. The tubulin−curcumin binding is characterized by simultaneous participation of favorable van der Waals (negative ΔH) and hydrophobic interactions (positive ΔS). The heat capacity change at constant pressure (ΔC_p) was also determined using Kirchoff's equation as $\Delta C_p = d\Delta H/dT$. A plot of enthalpy change (ΔH) of curcumin−tubulin binding as a function of temperature

Table 3. Heat Capacity Change of Tubulin−Curcumin Interaction

temperature (K)	ΔH (cal mol^{-1})	ΔS (cal K^{-1} mol^{-1})	ΔCp (cal K^{-1} mol^{-1})
293	−1154	20.7	−554.6
298	−5917	7.4	
303	−6624	4	

yielded ΔC_p = −554.6 cal/(mol K) (Table 3). In general, ΔC_p is negative for drug−protein and protein−protein interactions. This happens due to the removal of water from the protein surface.[26] A negative value of ΔC_p, associated with curcumin binding, indicates a surface−surface interaction between the protein and the drug. Calorimetric titration also revealed that half-curcumin analogues, compounds **9**−**13**, do not bind to tubulin. The entropic contribution associated with the binding reaction can be expressed as the sum of three terms.[27]

$$\Delta S_{tot} = \Delta S_{solv} + \Delta S_{conf} + \Delta S_{r/t} \quad (1)$$

where ΔS_{solv} describes the change in entropy resulting from solvent release upon binding, the ΔS_{conf} is the configurational term reflecting the reduction of rotational degrees of freedom around torsion angles of proteins and ligand, and $\Delta S_{r/t}$ describes the loss of translational and rotational degrees of freedom when a complex is formed from two molecules free in solution. The numerical value of $\Delta S_{r/t}$ is always close to the critical entropy of −8 cal K^{-1} mol^{-1}.[28]

ΔS_{solv} can be expressed at a given temperature (T) by following equation.

$$\Delta S_{solv} = \Delta C_p \ln\left(\frac{T}{T_s^*}\right) \quad (2)$$

Where, T_s^* is the temperature at which there is no solvent contribution to the hydrophobic entropy change and is equal to 112 °C (385 K).[29] Using ΔC_p = −554.6 cal/(mol K), T = 303 K, and T_s^* = 385 K, a value of 132.8 cal K^{-1} mol^{-1} is obtained for ΔS_{solv}. The observed positive change in solvation entropy is attributed to solvent reorganization. As a rule of thumb, desolvation entropy is always favorable (positive) and is the predominant force that drives binding of hydrophobic patch mediated protein−ligand association. Finally, the configurational entropy ΔS_{conf} is calculated from the following equation.

$$\Delta S_{conf} = \Delta S_{tot} - S_{solv} - S_{r/t} \quad (3)$$

The conformational entropy change is always unfavorable in protein−ligand binding event, as the binding process involves the loss of configurational degrees of freedom for both the drug molecule and the protein molecule, resulting in a negative change in conformational entropy. The unfavorable effect can be minimized by introducing conformational constraint in the drug molecule.[30] For curcumin−tubulin binding, the change in conformational entropy is −120.8 cal·K^{-1} mol^{-1}. The large change in conformational entropy is attributed to the flexible nature of curcumin. It is evident from the above discussion that the unfavorable conformational entropy change is overcompensated by a large favorable solvent contribution that leads to a small entropic gain.

Inhibition of Tubulin Polymerization by Curcumin Analogues. Curcumin and its analogues effectively inhibit the self-assembly of tubulin, with half-maximum polymerization inhibition

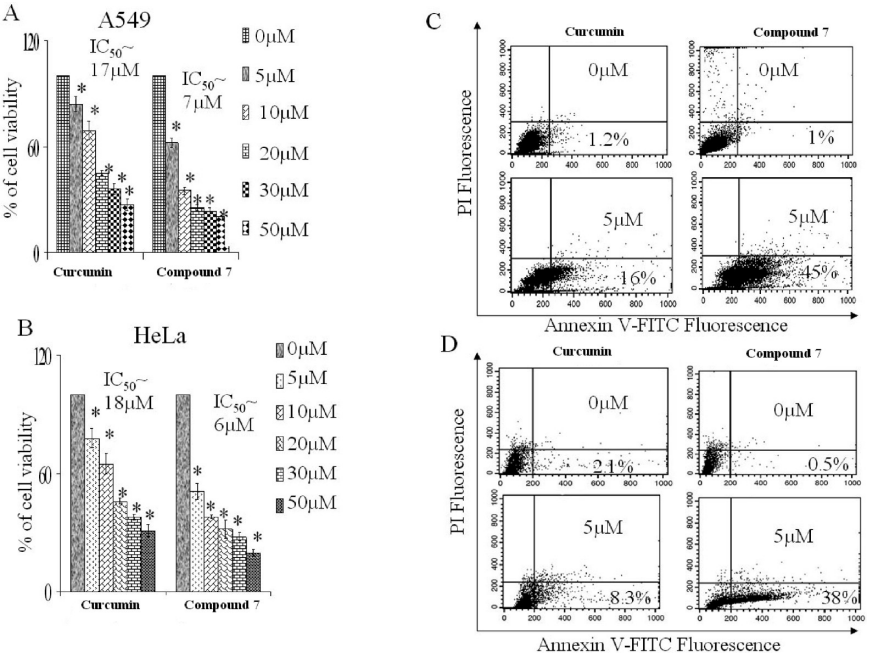

Figure 4. Inhibition of proliferation and induction of apoptosis in the cultured A549 and HeLa cells upon treatment with curcumin and compound 7. (A) Loss of viability of A549 cells with the increasing concentrations of curcumin and compound 7 (0−50 μM), when incubated for 48 h. Cell viability was assessed by MTT assay. (B) Loss of viability of HeLa cells with the increasing concentrations of curcumin and compound 7 (0−50 μM), when incubated for 48 h as assessed by MTT assay. Data are represented as mean ± SEM (*$P < 0.05$) (untreated cell) vs treated cells where $n = 4$. (C) Dot plot representation of Annexin-V-FITC-fluorescence (x-axis) vs PI-fluorescence (y-axis) of the apoptotic A549 (Annexin-V positive) cells, treated with curcumin and compound 7 (0−5 μM) for 48 h. (D) Dot plot representation of Annexin-V-FITC-fluorescence (x-axis) vs PI-fluorescence (y-axis) of the apoptotic HeLa (Annexin-V positive) cells, treated with curcumin and compound 7 (0−5 μM) for 48 h.

values ranging from 16 to 60 μM. We estimated the half-maximum polymerization inhibition values by studying the concentration dependent inhibition behavior of each drug against tubulin self-assembly (Figure S1, Supporting Information 1). Compound 7 was found to be the most effective in inhibiting tubulin polymerization with a half-maximum polymerization inhibition value of 16 ± 1 μM, whereas the half-maximum polymerization inhibition value of curcumin and compound **8** were 20 ± 1 and 60 ± 2 μM, respectively (Table 1). These three compounds (curcumin, compounds 7 and **8**) were also spectroscopically alike (and different from the others) in terms of their absorbance and fluorescence λ_{max} (Figure 1). The half-maximum polymerization inhibition values seem to increase when the diketone group of curcumin is modified leading to the breakdown of the extended conjugation across the molecule. (Table 1)

Cell-Based Study to Compare Potency of Curcumin and Compound 7. *Inhibition of Cell Proliferation and Delay Release of Cells from Mitotic Block.* The effect of curcumin and its analogue, compound 7, on proliferation of human lung epithelium cancer (A549) cells and human cervical cancer (HeLa) cells was assessed by MTT assay (described in Experimental Methods). The dietary antioxidant curcumin, and its analogue, compound 7, inhibited the proliferation of the A549 and HeLa cells after 48 h of incubation, in a concentration-dependent manner. From the results of the MTT assay, it was found that compound 7 was much more effective than curcumin. When treated with curcumin the IC_{50} (50% inhibitory concentration) value for A549 was around 17 ± 1.6 μM, while for the HeLa cells, it was around 18 ± 1 μM, respectively. On the other hand, when the cells were treated with compound 7, IC_{50} value for A549 was around 7 ± 0.4 μM, while for the HeLa cells, it was around 6 ± 0.8 μM, respectively (Figures 4A,B). To investigate whether treatment of curcumin and its derivative, compound 7, resulted in a G_2/M block in cell cycle, we first performed the cell cycle analysis with the HeLa cells, being treated with 5 μM of both the compounds for 24 h. No blockages of the cell cycle progression in the treated HeLa cells were observed in the G_2/M phase (data not shown). This result is consistent with that observed and reported by Banerjee et al.,[20] where it was reported that treatment with curcumin does not cause any cell cycle arrest in the MCF-7 cells but potentially inhibits the release of the cells from the mitotic block induced by nocodazole.[20] To check whether compound 7 also inhibits the release of cells from mitotic phase of the mammalian cells induced by nocodazole, cell cycle analysis of the nocodazole treated HeLa cells was performed in the presence of both curcumin and compound 7 (Figure S2, Supporting Information). The HeLa cells were treated with nocodazole (1.5 μM) for 20 h, which resulted in their accumulation in the M phase of the cell cycle. Then the cells were washed with fresh medium and subsequently incubated in medium with and without curcumin and compound 7 (5 μM each) separately. Nocodazole treatment resulted in the accumulation of 38% of the cells in the G_2/M phase, while in the untreated cells the mitotic population was only 6%. After the removal of the nocodazole containing medium, and incubation in the fresh medium for 8 h, the G_2/M population decreased to 12%, suggesting the release of the cells from nocodazole induced mitotic block. Interestingly, when the nocodazole treated HeLa cells were incubated in the presence of 5 μM of compound 7 for 8 h after removing nocodazole, 35% of the cells were found to be in the G_2/M phase of the cell cycle, but in the presence of 5 μM curcumin, only 18% of the cells were found to be in the G_2/M phase. These

dx.doi.org/10.1021/jm2004046 |J. Med. Chem. 2011, 54, 6183–6196

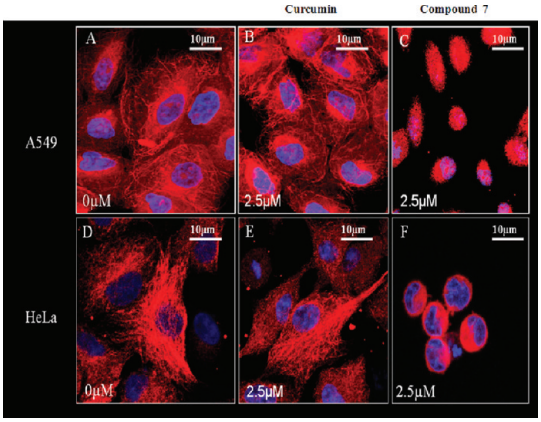

Figure 5. Disruption of microtubule network in the cultured A549 and HeLa cells upon treatment with curcumin and compound 7. Cultured A549 and HeLa cells were incubated in the presence of varying concentrations of curcumin and compound 7 for 24 h. The samples were stained for immunofluorescence using mouse monoclonal anti-α-tubulin antibody and corresponding rhodamine conjugated (red) secondary antibody. Microtubule images of the control and treated A549 cells (A−C) and HeLa cells (D−F) were taken under a Ziess confocal microscope (LSM 510 Meta). The results represent the best of data collected from three experiments with similar results (n = 3).

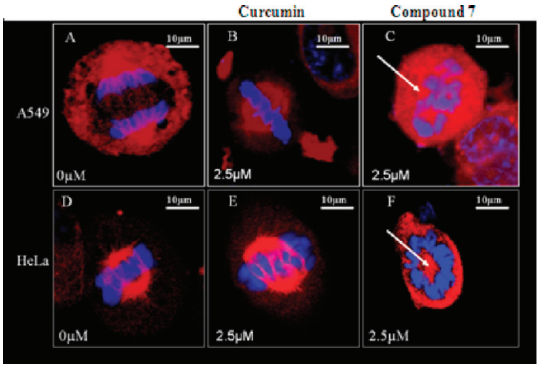

Figure 6. Effects of curcumin and compound 7 on spindle microtubules and chromosome organization of A549 and HeLa cells. Cultured A549 and HeLa cells were incubated in the presence of varying concentrations of curcumin and compound 7 (0−2.5 μM) for 24 h. The spindle microtubules were stained for immunofluorescence using mouse monoclonal anti-α-tubulin antibody and corresponding rhodamine conjugated (red) secondary antibody and the chromosomes were stained with DAPI (blue). Images of the spindle microtubule in the control and treated A549 cells (A−C) and HeLa cells (D−F) were taken under a Ziess confocal microscope (LSM 510 Meta). The results represent the best of data collected from three experiments with similar results (n = 3).

results clearly indicated that compound 7 inhibited the release of cells from mitotic phase induced by nocodazole much more effectively than curcumin.

Induction of Apoptosis. To compare the abilities of compound 7 and curcumin to induce apoptosis in mammalian cancerous cell lines, FITC conjugated annexin-V/PI assay was performed with both A549 and HeLa cells. After 48 h of treatment, the extent of apoptosis in both cell lines was higher in the case of compound 7 as compared to curcumin (Figures 4C,D). About 16% of cells were found to be apoptotic (annexin-V positive) in the A549 cells when treated with 5 μM curcumin for 48 h, while under the same concentration of compound 7, about 45% of the A549 were subjected to apoptosis (Figure 4C). Similarly, treatment of the HeLa cells with 5 μM curcumin resulted in only 8% of the apoptotic cells. But when treated with 5 μM of compound 7, about 38% of the HeLa cells were found to be apoptotic (Figure 4D).

Further, it was also found that treatment with 5 μM of compound 7 resulted in the aberration and fragmentation of the nuclear DNA of both A549 and HeLa cells as monitored by the DAPI staining, but at the similar dose of curcumin, the nucleus of the cultured cells remained unaffected (Figure S3, Supporting Information).

Disruption of Interphase Microtubule and Morphological Aberrations. To observe the effect of curcumin and compound 7 on the morphology of A549 and HeLa cells, phase contrast images of the control and treated cells were recorded after 24 h of incubation. Phase contrast images of the treated A549 and HeLa cells indicated that their regular morphologies were altered in a dose-dependent fashion when incubated with compound 7. At 2.5 μM of compound 7, shrinkage of the cells were found to be initiated after 24 h of incubation, and at a dose of 5 μM, the cells were found to be contracted and rounded, but when the cells were incubated with similar concentrations of curcumin, no significant alteration of the cellular morphology was observed (Figure S4, Supporting Information).

To investigate whether compound 7 is perturbing the cellular microtubules, and hence resulting in the cellular contraction, the status of the interphase microtubule network in the treated A549 and HeLa cells was monitored. Confocal microscopic studies revealed that compound 7, but not curcumin, is effective in disrupting the microtubule network of both the A549 and HeLa cells in a dose-dependent fashion at a lower range of concentrations. The interphase microtubules exhibited fibrous network-like structures in the untreated A549 cells (Figure 5A), but when incubated with 2.5 μM of compound 7, the microtubules were completely depolymerized (Figure 5C). However, when the cells were treated with the same concentrations of curcumin, no significant damage of the microtubule network was observed (Figure 5B).

Similar trend was observed when the HeLa cells were treated with 2.5 μM of compound 7. Intact microtubule network, as observed in the untreated cells (Figure 5D), were found to be distorted upon treatment with 2.5 μM of compound 7 (Figure 5F), but the microtubule damage was not severe when the HeLa cells were treated with 2.5 μM curcumin (Figure 5E). These results clearly indicated that compound 7 is a much more potent antimicrotubule agent than curcumin.

Perturbation of Spindle Microtubule and Chromosomal Organization. It has been reported that curcumin inhibits mitosis and perturbs spindle microtubule organization in the cancer cell lines (HeLa and MCF-7) at a concentration of 10−36 μM.[19] To follow up this observation, we investigated the effect of both curcumin and compound 7 on spindle microtubules of both A549 and HeLa cells at lower concentrations. In the untreated A549 cells, normal bipolar spindles were observed with chromosomes congregated in the form of compact metaphase plates (Figure 6A). At 2.5 μM, curcumin showed no significant effect on spindle microtubules (Figures 6B), but when the cells were treated with similar concentrations of compound 7, spindle microtubules were disorganized and accompanied by misaligned chromosomes from the metaphase plate (Figures 6C).

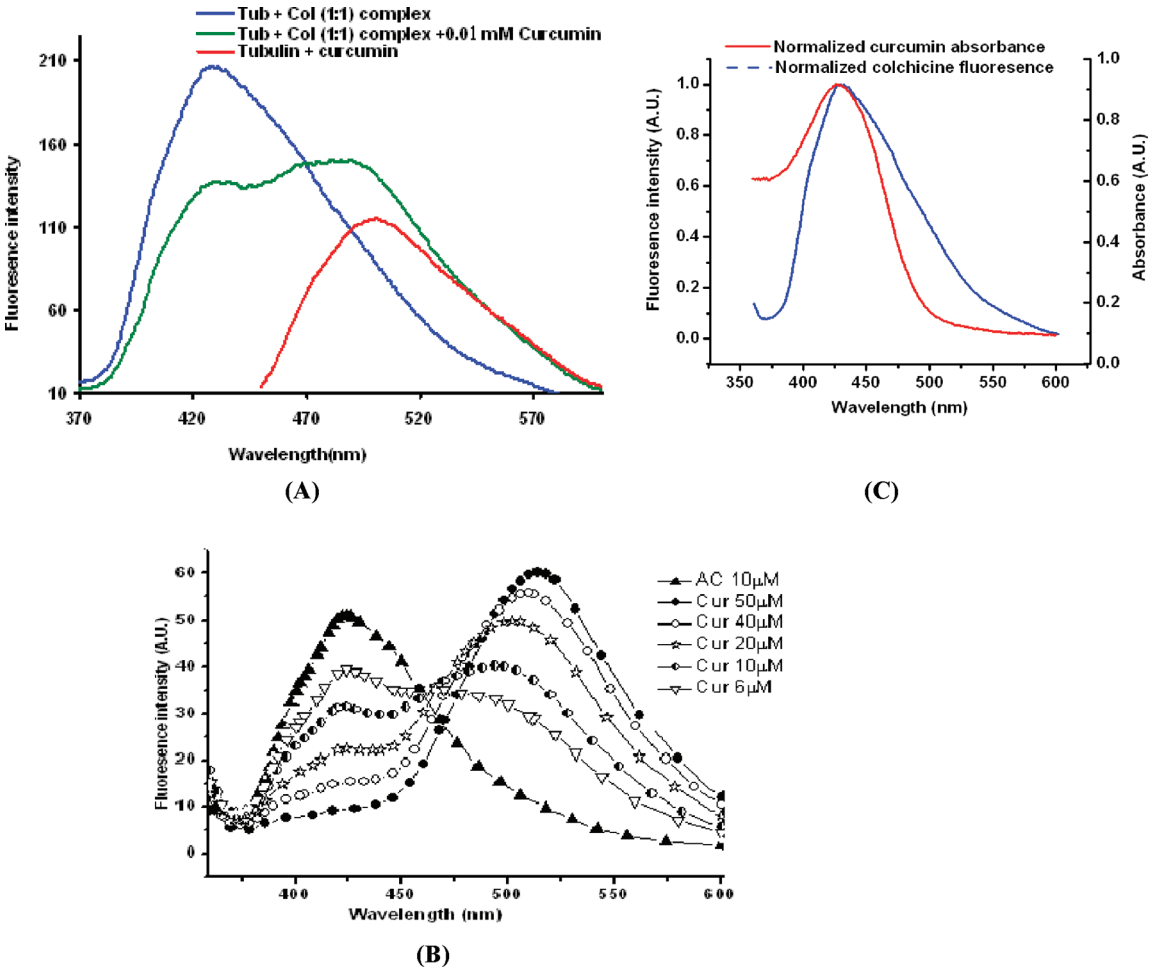

Figure 7. Determination of the Forster distance for tubulin-bound colchicine and curcumin. (A) Energy transfer from tubulin-bound colchicine to tubulin-bound curcumin. The blue curve is the emission spectrum colchicine−tubulin complex (1:1, each of 5 μM). The excitation wavelength was the absorbance maxima of colchicine (350 nm). The temperature was kept at 30 °C. The green curve is the emission spectrum of the colchicine−tubulin complex in the presence of 10 μM curcumin. (B) Energy transfer from tubulin-bound AC analogue of colchicine to tubulin-bound curcumin. (C) The spectral overlap between the emission (λ_{ex} = 350 nm) of the donor (tubulin−colchicine complex) and the absorption spectrum of the acceptor (tubulin−curcumin) complex, R_o of 28 Å, was calculated for the donor−acceptor pair.

Similar results were observed when the cultured HeLa cells were treated with curcumin and compound 7. Treatment of the HeLa cells with 2.5 μM of curcumin did not significantly perturb the spindle microtubule organization (Figures 6E). However, when the cells were treated with similar concentrations of compound 7, perturbation of the spindle microtubules was observed (Figures 6F).

DISCUSSION

Although the above experimental data clearly shows that curcumin and compound 7 bind tubulin with high affinity, their exact binding site in tubulin still remains elusive. To gain some insights into the possible binding site of curcumin, FRET experiments and docking studies were performed. In addition, structure−activity relationship (SAR) was investigated among structurally diverse curcumin analogues.

Localization of the Curcumin-Binding Site on Tubulin Using FRET Experiments. The weak fluorescence of colchicine in aqueous medium becomes much stronger upon binding to tubulin (λ_{ex} = 350 nm, λ_{em} = 427 nm; Figure 7A). When curcumin was added to a mixture of colchine-bound tubulin, colchicine fluorescence decreased with a concomitant increase in the fluorescence emission of curcumin (λ_{em} = 500 nm) (Figure 7A). Because binding of colchicine to tubulin is poorly reversible, the same experiment was repeated with a colchicine analogue, compound AC (2-methoxy-5-(2′,3′,4′-trimethoxyphenyl)-tropone), lacking the colchicine B-ring. The AC analogue binds tubulin at the colchicine-binding site in a reversible manner (Figure 7B, Figure S5, Supporting Information). It was observed that the fluorescence intensity of ligand−tubulin complex decreases and the associated tubulin-curcumin fluorescence increases more efficiently with AC analogue as the ligand compared to when colchicine is the ligand. There are two scenarios that can give rise to the observed concomitant decrease of tubulin-bound colchicine/AC analogue fluorescence and increase of tubulin-bound curcumin fluorescence as colchicine/AC analogue-bound tubulin is titrated with curcumin. Either both curcumin and colchicine/AC analogue bind at the same binding site and addition of curcumin replaces colchicine/AC analogue from the binding site into the bulk, thus reducing their fluorescence, or curcumin binds at a binding site other than the colchicine-binding site but quenches colchicine/AC analogue

dx.doi.org/10.1021/jm2004046 |J. Med. Chem. 2011, 54, 6183–6196

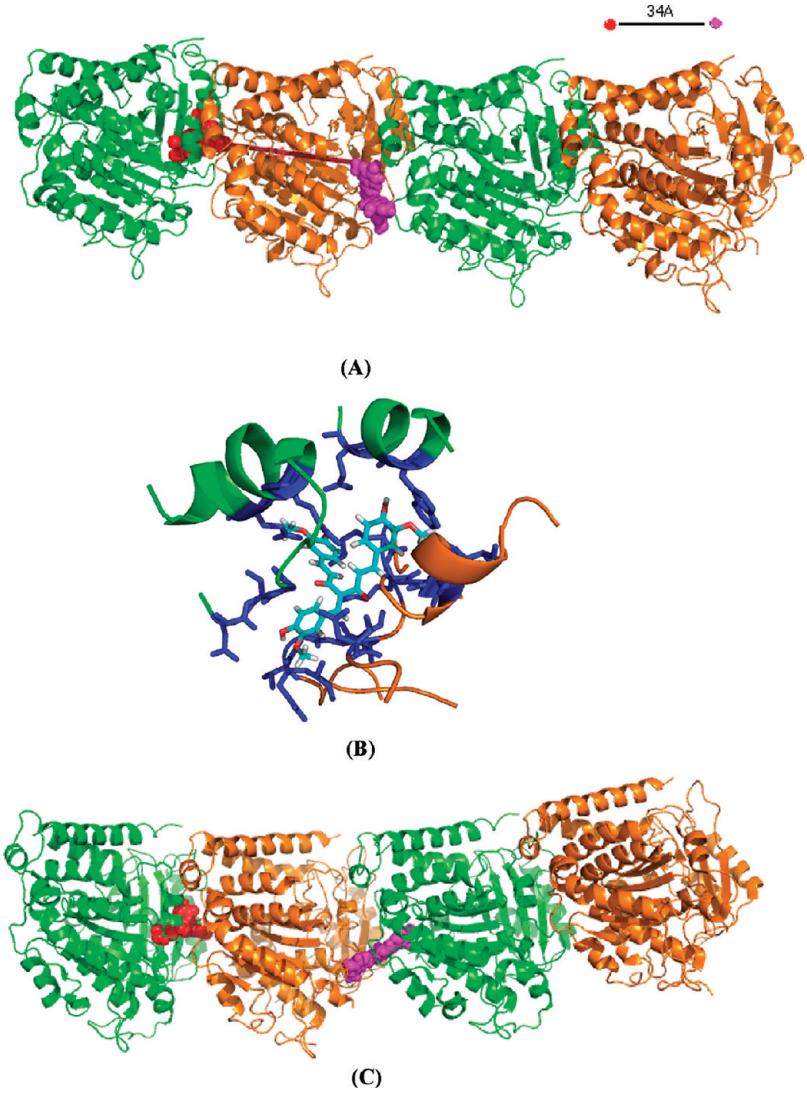

Figure 8. Molecular modeling of compound **7** (A) and curcumin bound tubulin (C) complex, the ligands curcumin and compound **7** (in magenta) were placed between two $\alpha\beta$-heterodimers (α in orange, and β in green) and colchicine in red. (B) The local environment of compound **7** (in cyan) with a few functionally important residues shown in blue.

fluorescence by FRET (curcumin absorbance and colchicine/AC analogue fluorescence show significant overlap).

If the observed colchicine/AC analogue fluorescence quenching indeed arises due to competitive binding between curcumin and colchicine/AC analogue, the addition of a suitable curcumin analogue, incapable of participating in FRET with tubulin-bound AC analogue, would still quench the fluorescence of tubulin-bound AC analogue. We performed this experiment with compound **2** as the curcumin analogue because it exhibits insignificant overlap with the emission spectrum of tubulin-bound AC analogue, ruling out any potential FRET between the two. In addition, unlike the parent compound curcumin, the molar extinction coefficient of compound **2** is negligible compared to the AC analogue above 375 nm, ruling out direct excitation. We did not notice any fluorescence quenching (λ_{ex} = 380 nm) of the AC analogue when compound **2** was added to tubulin-bound AC analogue (Figure S6, Supporting Information), establishing that compound **2** (and by extrapolation, curcumin) does not bind to the colchicine-binding site of tubulin.

Having ruled out the binding of colchicine/AC analogue and curcumin at the same binding site, we estimated the distance between tubulin-bound colchicine and curcumin from FRET studies. The emission spectrum of tubulin-bound colchicine and the absorption spectrum of curcumin show substantial overlap (Figure 7C), making the pair amenable to FRET studies. The characteristic Forster distance for the pair was estimated as 28 Å (using $\kappa^2 = 2/3$, $n = 1.336$, and $Q_D = 0.03$, the overlap integral J was estimated as 8.5×10^{-14} M^{-1} cm^3). Using this value of R_o (28 Å), the distance between tubulin-bound colchicine and tubulin-bound curcumin was estimated as 32 Å. Strictly speaking, donor−acceptor distance can be estimated from FRET experiments by the above method only when the acceptor shows no absorption at the λ_{ex}. In our case, curcumin shows a shoulder at λ_{ex} (350 nm). To circumvent this problem, we also estimated the FRET efficiency for the colchicine−curcumin pair using an alternate method that can exclude artifacts arising from the overlap between acceptor and donor absorption spectra.[31] The estimated energy transfer efficiency (20%) was close to that obtained using the direct method.

dx.doi.org/10.1021/jm2004046 |*J. Med. Chem.* 2011, 54, 6183–6196

In summary, using FRET measurements, we have shown that curcumin and its analogue, compound **2**, do not bind tubulin at the colchicine-binding site. The binding site is about 32 Å away from the colchicine-binding site. Among other canonical binding sites on tubulin, the vinblastine-binding site approximately satisfies this distance constraint. Unfortunately, we failed to perform any direct binding assay (competition experiment) between curcumin and vinblastine as both the ligands induce tubulin aggregation (data not shown).

Molecular Modeling of Compound 7 Binding Site on Tubulin. FRET experiment clearly showed that curcumin binds tubulin about 32 Å away from the colchicine-binding site. To confirm the FRET results, molecular docking was performed to locate the probable binding site of compound **7** on tubulin.

In the docked structure, compound **7** binds at the interdimer interface, between the α and the β-subunits of two α,β-dimers, close to the vinblastine binding site (Figure 8A). Residues 96−98 from the β-subunit and 251−256 from the α-subunit constitute the binding site. The pocket also contains H3′-helix (residues 105−110), T4 and T5 loops (residue 130−133 and 163−165), and the end of helix H11′ (residues 407−411).[32] The longitudinal contacts between neighboring monomers in a microtubule are mostly mediated through residues 251−256 (end of T7 loop and the beginning of H8 helix).[33] Both the T5 and T7 loops are highly dynamic in nature and can accommodate a variety of ligands by changing their conformational state. Tubulin−compound **7** interaction is mainly stabilized by van der Waals contacts, although the involvement of hydrophobobic stacking interactions between the phenyl ring of compound **7** and the aromatic rings of β-Trp 407 was also observed (Figure 8B). Interestingly, the calculated distance (34 Å) between colchicine and compound **7** is quite close to the experimentally determined distance (32 Å). Molecular modeling of curcumin on tubulin also reveals that both curcumin and compound **7** shares a close binding site. (Figure 8C)

Structure−Activity Relation of Curcumin−Tubulin Interaction. Curcumin is a flexible molecule, consisting of two polyphenol rings connected to the ends of an α,β-unsaturated diketone moiety. The substitution of diketone with isoxazole, pyrozole, and substituted pyrozole produced compounds that showed weaker (than curcumin) inhibition behavior against tubulin polymerization, consistent with cell-based studies (data not shown). These results indicate that the diketone moiety participates in the binding interaction between curcumin and tubulin. The interaction between different curcumin analogues and tubulin has been studied using calorimetric as well as fluorescence spectroscopic techniques. The binding study by fluorescence spectroscopy identified two distinct groups within curcuminoids. Both compounds, **7** and **8**, have free diketone moieties and show structural resemblance with curcumin. Together, they also show a characteristic emission maxima at a much higher wavelength compared to the rest of the analogues. Additionally, compound **7**, which has a substituted polyphenol ring in between the dicarbonyl moiety, was found to be most effective in inhibiting tubulin self-assembly (half-maximum polymerization inhibition value 16 μM) and bound tubulin with a higher affinity compared to the parent compound curcumin (half-maximum polymerization inhibition value 20 μM). It is possible that the extra steric hindrance caused by the substitution of a polyphenol in between the diketones in compound **7**, compared to curcumin, makes compound **7** more conformationally constrained. As a result, compound **7** binding to tubulin is associated with less conformational entropy loss than binding of curcumin to tubulin. Substitution of a polyphenol ring in between the diketones also produces a tridentate molecule that can be anchored to tubulin with higher affinity. It is interesting to note that acetylation of the phenolic groups at the two termini of compound **8** produced an analogue which was less effective in inhibiting tubulin self-assembly (half-maximum polymerization inhibition value 60 μM), indicating their participation during binding to tubulin. The structure−activity relationship studies also emphasize the role of the diketone and the phenolic OH groups in compounds with biological activity. The half molecules of curcumin (compounds **9**−**13**) were inactive in binding tubulin as revealed by ITC, indicating that curcumin acts as a bifunctional ligand when it binds to tubulin. Recently, Qui et al. have shown[18] that arylidene curcumins are more potent anticancer agents than curcumin. These drugs are reported to inhibit TNF-α mediated NF-$\kappa\beta$ activation. Our observations reveal that curcumin and benzylidene analogues of curcumin target tubulin in both in vitro as well as in cell culture experiments. Compelling evidence are available regarding the role of microtubules as an upregulator of TNF-α mediated NF-$\kappa\beta$ signal transduction and gene expression.[34] It is known that microtubule depolymerization triggers deactivation of NF-$\kappa\beta$ signal transduction, suggesting that by blocking tubulin polymerization, curcumin analogue can deactivate the NF-$\kappa\beta$ mediated signal transduction pathway.[35] The data presented here comprehensively show that curcumin analogues arrest cancer cell proliferation by binding to tubulin.

CONCLUSION

In this report, we have established that tubulin is one of the targets of curcumin and elucidated the SAR between tubulin and curcumin derivatives. The binding site of curcumin in tubulin has been ascertained from both experimental and modeling studies. In summary, the enhanced activity of the benzylidene analogues of curcumin is attributed to their higher binding affinity toward tubulin. Further modifications of benzylidene analogues may lead to alterations in their binding affinity and associated anticancer activity.

EXPERIMENTAL METHODS

Piperazine-*N*,*N*′-bis(2-ethanesulphonic acid) (PIPES), guanosine-5′-triphosphate (GTP), ethylene glycol-bis(β-aminoethyl ether) *N*,*N*,*N*′,*N*′-tetraacetic acid (EGTA), PMSF, demcolchicine, and vinblastine were purchased from Sigma Chemical Co. All other reagents were of analytical grade.

Chemistry. *Synthesis of Compounds* ***1***−***13***. All reagents and solvents used were purchased from the best available commercial sources. Melting points were determined with Barnstead electrothermal apparatus and are uncorrected. Mass spectra were recorded on Micromass LCT kc 436 mass spectrometer using a Waters 1525 binary pump. All compounds were more than 99% pure as determined by Shimadzu LC-20AT HPLC system (Figure S7, Supporting Information). The HPLC analyses were performed on Phenomenex C_{18} column (250 mm × 4.6 mm, 5 μm). The optimum HPLC separation was achieved on isocratic mode with a mobile phase composed of methanol, acetonitrile, and 0.6% acetic acid aqueous solution (25:20:55, v/v/v) at a flow rate of 0.5 mL min^{-1}. ^1H and ^{13}C NMR spectral analyses were performed on Bruker Avance 300 MHz spectrometer with tetra-methylsilane as the internal standard (δ ppm). The following abbreviations were used to explain the multiplicities: s, singlet; d, doublet; t, triplet; dd, double

Scheme 1. Synthesis of Cinnamic Acids from Acetic Acid and Substituted Benzalaldehydes (IIa−b, IIIc−e)[a]

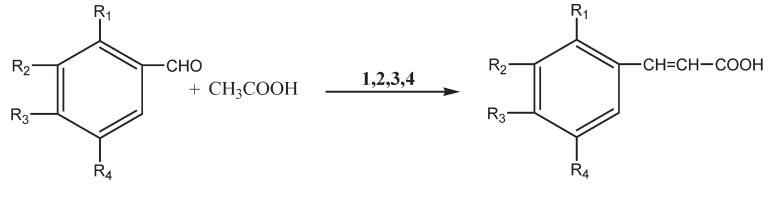

I II

Reactant	R1	R2	R3	R4
a	H	H	H	H
b	H	OCH_3	OCH_3	H
d	OCH_3	H	H	H
e	OCH3	H	OCH_3	H

Product	R1	R2	R3	R4
a	H	H	H	H
b	H	OCH_3	OCH_3	H
d	OCH_3	H	H	H
e	OCH3	H	OCH_3	H

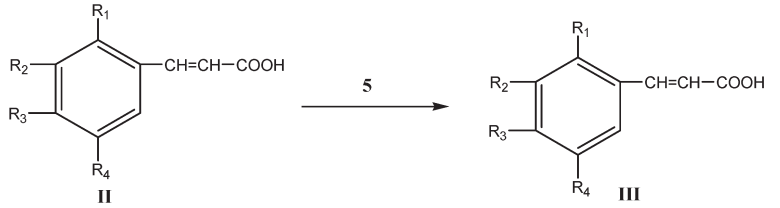

II III

Reactant	R1	R2	R3	R4
b	H	OCH_3	OCH_3	H
d	OCH_3	H	H	H
e	OCH3	H	OCH_3	H

Product	R1	R2	R3	R4
c	H	OH	OH	H
d	OH	H	H	H
e	OH	H	OH	H

[a] Reagents and Conditions: (1) BBr_3, benzene, 55−65 °C, 5−6 h; (2) 4-DMAP, pyridine, NMP, 20−30 °C; (3) *substituted benzaldehyde*, 180−190 °C; (4) 20% HCl; (5) BBr_3/DCM, −78°C to rt.

doublet; m, multiplet, br,broad. Solvents and reagents were purified according to standard laboratory techniques.

*Synthesis of Curcumin Analogues (**1**−**8**).* The detailed synthetic methods of curcumin analogues **1**−**8** are reported by us in our earlier publication.[25]

*Synthesis of 3-Phenylprop-2-enoic Acid (**9**).* Anhydrous acetic acid (6.3 mL, 0.1089 M) was added to a 100 mL three-necked round-bottomed flask equipped with thermometer and water cooled reflux condenser. Boron tribromide (2.2 mL, 0.022 M) in anhydrous benzene (5 mL) was gradually added to the above solution in 30 min at 0−4 °C. The reaction mixture was allowed to stir for an hour at room temperature and further for 5−6 h at 55−65 °C to expel hydrogen bromide gas. When the gas emission ceased, a solution of triacetyl borate in benzene and acetic acid was obtained. Benzene and acetic acid were distilled off from the reaction mixture. The resulting residue was cooled to 20−30 °C, and DMAP (1.3 g, 0.01M), pyridine (2.412 mL, 0.03M), and NMP (2 mL) were added successively while stirring. Benzaldehyde (**Ia**) (2.03 mL, 0.02 M) was then added to this reaction mixture containing triacetyl borate, which was stirred for 5 min followed by refluxing for 12 h. The resulting mixture was diluted with water (70−80 mL) and pH of the solution adjusted to 9−10 with 20% NaOH solution. The unreacted benzaldehyde was removed by distillation with water under vacuum (30−40 mm of Hg). Water was added to the resulting residue and cooled to room temperature, stirred, and filtered. The filtrate was brought to pH 1−2 with 20% HCl solution to precipitate out cinnamic acid. The filtrate was stirred for 2 h at 0−4 °C. The product was filtered, washed with ice-cold water (15−20 mL), and dried to yield crude cinnamic acid (**IIa**). The crude product was recrystallized from hot water (yield 1.93 g, 65%; mp 132−135 °C (Scheme 1)).[36]

*Synthesis of 3-(3,4-Dimethoxyphenyl)prop-2-enoic Acid (**10**).* In situ generated triacetyl borate, as synthesized above, in benzene and acetic acid was cooled to 20−30 °C and DMAP (1.3 g, 0.01 M), pyridine (2.412 mL, 0.03M), and NMP (2 mL) were added to it while stirring. To the above mixture, 3,4-dimethoxybenzaldehyde (**Ib**) (3.32 g, 0.02 M) was added stirred for 5 min. Benzene and acetic acid were removed by distillation from the reaction mixture. The residue was heated at 180−190 °C for 9 h and was further subjected to the series of treatments described earlier for **9** to obtain crude 3,4-dimethoxycinnamic acid (**IIb**). Recrystallization from hot water yielded pure compound (yield 2.08 g, 50%; mp 181−183 °C (Scheme 1)).

*Synthesis of 3-(3,4-Dihydroxyphenyl)prop-2-enoic Acid (**11**).* 3,4-Dimethoxycinnamic acid (**IIb**) (0.0624 g, 0.3 mM) was dissolved in dry dichloromethane (3 mL) and cooled to −78 °C. A solution of BBr_3 in DCM (1 M) (2.0 mL) was added dropwise to the above solution. After the addition was over, the reaction mixture was brought to room temperature and stirred for 24 h. The reaction mixture was diluted with ethyl acetate and its pH was adjusted to ∼8 with aqueous NaOH, and the layers were separated. The organic layer was washed with water and brine solution, dried over anhydrous Na_2SO_4, and vacuum evaporated. The crude product was further purified by column chromatography using silica gel (60−120 mesh size) with a 1:5 mixture of ethyl acetate and hexane to give of caffeic acid (**IIIc**) (yield 1.60 g, 44%; mp 223−225 °C (Scheme 1)).

*Synthesis of 3-(2-Hydroxyphenyl)prop-2-enoic Acid (**12**).* DMAP (1.3 g, 0.01M), pyridine (2.412 mL, 0.03 M), and NMP (2 mL) were added to triacetyl borate generated in situ in benzene and acetic acid (described for **IIa**) at 20−30 °C. 2-Methoxybenzaldehyde (**1d**) (2.72 g, 0.02 M) was added to the above mixture and stirred for 5−10 min, followed by distillation of benzene and acetic acid from the system. The resulting residue was heated at 180−190 °C for 9 h and was further subjected to the series of treatments described for **IIa** to obtain 2-methoxycinnamic acid (**IId**). The crude product was recrystallized

dx.doi.org/10.1021/jm2004046 |*J. Med. Chem.* 2011, 54, 6183–6196

from hot water with a melting point of 182−186 °C. 2-Methoxycinnamic acid (**IId**) (0.0534 g, 0.3 mM) thus synthesized was subjected to demethylation as described earlier for **IIIc** to obtain of 2-hydroxy cinnamic acid (**IIId**) (yield 1.80 g, 54%; mp 217 °C, (Scheme 1)).

*Synthesis of 3-(2,4-Dihydroxyphenyl)prop-2-enoic Acid (**13**).* To a solution of triacetyl borate (generated in situ) in benzene and acetic acid (as described for (**IIa**) at 20−30 °C, DMAP (1.3 g, 0. 01 M), pyridine (2.412 mL, 0.03 M), and NMP (2 mL) were added. 2,4-Dimethoxy benzaldehyde (**Ie**) (3.32 g, 0.02 M) was added to it, and the system was stirred for 5−10 min. This reaction mixture was then subjected to the steps described earlier for the synthesis of **IIa**, which eventually yielded 2,4-dimethoxycinnamic acid (**IIe**). The melting point of **IIe** after recrystallization from hot water was 192−194 °C. 2,4-Dimethoxycinnamic acid (**IIe**) was then taken through the demethylation procedure described for the compound **IIIc** to obtain 2,4 dihydroxycinnamic acid (**IIIe**) (yield 1.60 g, 44%; mp 201−203 °C (Scheme 1)).

*3-Phenylprop-2-enoic Acid (**9**).* λ_{max}(MeOH): 273 nm. Retention time (t_R) in the reverse phase HPLC (RP-HPLC) carried out as described for compound **9**: t_R = 20.38 min. δ_H (300 MHz, $CDCl_3$) 7.8 (1H, d, J = 16.2 Hz), 7.41−7.38 (5H, m), 6.45 (1H, d, J = 15.9 Hz). δ_C (75.4 MHz, $CDCl_3$) 172.7, 147.0, 133.7, 132.5, 130.5, 127.91, 128.8, 128.2, 117.0. ESI-MS m/z: calculated for $C_9H_8O_2$: 148.05. ESI-MS m/z (−ve mode) found: [(M − H) + $2H_2O$-H] as precursor to product ion transition with m/z 180.95 adduct during ionization process. A dimeric structure of the above ion predominated the spectrum with m/z 362.8. Analysis (CHN) Found: C, 72.96%; H, 5.4%. Calculated: C, 72.94%; H, 5.44% (Figure S7, Supporting Information) .

*3-(3,4-Dimethoxyphenyl)prop-2-enoic Acid) (**10**).* λ_{max} (MeOH): 285 nm. RP-HPLC t_R = 13.87 min. δ_H (300 MHz, DMSO) 7.46 (1H, d, J = 15.9 Hz), 7.09 (1H, J = 1.8 Hz), 7.15 (1H, dd, J = 8.4, 2.4 Hz), 6.9 (1H, d, J = 8.4 Hz), 6.3 (1H, d, J = 15.9 Hz), 3.72 (3H, d, J = 15 Hz). δ_C (75.4 MHz, DMSO) 169.4, 151.5, 149.6, 145.5, 127.6, 123.6, 117.0, 112.3, 110.9, 56.3. ESI-MS m/z: calculated for $C_{11}H_{12}O_4$: 208.2. ESI-MS m/z (−ve mode) found: a prominent signal at m/z 254 was due to [(M − H) + (−OH) + ($-OCH_3$)] as precursor. CHN analysis Found: C = 63.4%; H = 5.85%. Calculated: C = 63.45%; H = 5.81% (Figure S7, Supporting Information) .

*3-(3,4-Dihydroxyphenyl)prop-2-enoic Acid) (**11**).* λ_{max} (MeOH): 320 nm. RP-HPLC t_R = 7.56 min. δ_H (300 MHz, DMSO): 7.40 (1H, d, J = 15.6 Hz), 7.02 (1H, J = 1.8 Hz), 6.9 (1H, dd, J = 8.1, 1.8 Hz), 6.75 (1H, d, J = 8.1 Hz), 6.18 (1H, d, J = 15.9 Hz). δ_C (75.4 MHz, DMSO) 169.2, 148.3, 145.6, 125.2, 122.1, 116.2, 115.2, 114.9. ESI-MS m/z: calculated for $C_9H_8O_4$: 180.05. ESI-MS (−ve mode) found: three prominent signals at m/z 343, 397, and 451 were found that were probably due to dimerization and adduct formation. m/z = 343 [(dimer of cinnamaldehyde) + (−OH)-H)], m/z = 397 [(dimer of cinnamaldehyde) + 3(H_2O) + (−OH) −H]. CHN analysis Found: C = 60.00%; H = 4.48%. Calculated: C = 60.00%; H = 4.48% (Figure S7, Supporting Information) .

*3-(2-Hydroxyphenyl)prop-2-enoic Acid (**12**).* λ_{max} (MeOH): 321 nm. RP-HPLC: t_R = 12.37 min. δ_H (300 MHz, DMSO) 7.79 (1H, d, J = 16.2 Hz), 7.49−7.46 (1H, m), 7.2−7.1 (4H, q), 6.4 (1H, d, J = 6.4 Hz). δ_C (75.4 MHz, DMSO) 169.6, 157.2, 141.08, 133.08, 132.73, 129.62, 121.6, 120.7, 118.7, 117.02. ESI-MS m/z: calculated for $C_9H_8O_3$: 164.1. ESI-MS (−ve mode) found: [(M − H) + (−OH) + 2($-OCH_3$)] as precursor to product ion transition with m/z 242 adduct during ionization process. A dimeric structure of the above ion predominated the spectrum with m/z at 484. CHN analysis Found: C = 65.85%; H = 4.91%. Calculated: C = 65.85%; H = 4.91% (Figure S7, Supporting Information) .

*3-(2,4-Dihydroxyphenyl)prop-2-enoic Acid) (**13**).* λ_{max} (MeOH): 319 nm. RP-HPLC: t_R = 7.71 min. δ_H (300 MHz, DMSO) 7.72 (1H, d, J = 15.9 Hz), 7.32 (1H, d, J = 8.1 Hz), 6.5 (1H, s), 6.3 (1H, dd, J = 1.2, 8.4 Hz). δ_C (75.4 MHz, DMSO) 169.8, 160.8, 158.5, 141.0, 130.8, 114.2, 113.3, 108.4, 102.9. ESI-MS m/z: calculated for $C_9H_8O_4$: 180.05. ESI-MS (−ve mode) found: the main adduct appears due to a dimeric cinnamaldehyde quasimolecular ion, possibly associated with one water and three methanol molecules through hydrogen bonding at m/z 441. The other prominent adduct signals at m/z 230, 330, 417, 527, and 616 appear due to water and methanol molecules associated with monomer, dimer, and multimers in varying composition. CHN analysis Found: C = 60.00%; H = 4.44%. Calculated: C = 60.00%; H = 4.48% (Figure S7, Supporting Information).

Tubulin Isolation and Estimation. Microtubular proteins were isolated from goat brains by two cycles of a temperature-dependent assembly disassembly process. Pure tubulin was isolated from microtubular proteins by two additional cycles of temperature-dependent polymerization and depolymerization using 1 M glutamate buffer for assembly.[37] The composition of the assembly buffer was 50 mM PIPES, pH 7, 1 mM EGTA, 0.5 mM $MgCl_2$, and 0.5 mM GTP. The protein was stored at −80 °C. The protein concentration was determined by Lowry method using bovine serum albumin as standard. Tubulin preparations used in this study contained natural mixture of isoforms.[38] Both calorimetry and fluorescence measurements were carried out with this unfractionated tubulin, and therefore the binding parameters obtained here are averages for the different isoforms.

Tubulin Polymerization Assay. Pure tubulin in PEM (50 mM PIPES, pH 7, 1 mM EGTA, 0.5 mM $MgCl_2$) buffer was polymerized at 37 °C in the presence of 1 mM GTP. Polymerization was initiated using 10% dimethyl sulfoxide, and the turbidity was measured by the absorbance at 360 nm. A Shimadzu UV-160 double beam spectrophotometer, fitted with a temperature controlled circulating water bath accurate to ±0.2 °C, was used for this purpose. Half-maximum polymerization inhibition values were calculated using concentration of the drug that caused 50% inhibition of the polymer mass. Each test was performed in triplicate, and the half-maximum polymerization inhibition values reported represents the result of at least two repetitions. The slight difference in half-maximum polymerization inhibition values between our results and others could be due to slight variations in experimental conditions, drug purity, and solvent condition.

Fluorescence Measurement. The binding of the ligands to the protein was monitored by enhancement of curcumin fluorescence in the presence of tubulin. Fluorescence spectra were recorded using a Hitachi F-3000 fluorescence spectrophotometer connected to a constant temperature circulating water bath accurate to ±0.2 °C. All fluorescence measurements were carried out in a 0.5 cm path-length quartz cuvette, and fluorescence values were corrected for the inner filter effect using the following equation:

$$F_{cor} = F_{obs}\left\{\frac{\text{antilog}(A_{ex} + A_{em})}{2}\right\}$$

where A_{ex} and A_{em} are the absorbances of the ligand at the excitation and the emission wavelength. The complexes were excited at their characteristic wavelength maxima, which were 330 nm for compounds **2**−**6**, 427 nm for curcumin and compound **8**, and 370 nm for compound **7**. In all the experiment set up excitation and emission band-pass were 5 nm.

For small molecules binding to protein, the equilibrium between free and bound molecules is given by the equation[39]

$$\log\frac{(F_o - F)}{F} = \log K_b + n\log[Q]$$

where F_o and F denotes the steady-state fluorescence intensities in the absence and in the presence of the quencher (compound **7** and curcumin); K_b is the binding constant, n is the number of binding sites, and [Q] is the concentration of compound **7** and curcumin, respectively.

Isothermal Titration Calorimetry (ITC). ITC measurements were performed on a VP-ITC Micro Calorimeter of Micro Cal Inc., (MA, USA). Tubulin was dialyzed extensively against PEM buffer with

GDP (to offer stabilization) and the ligand (curcumin and its half analogue) dissolved in the last dializant. The pH of the tubulin and the ligand solutions was made identical before loading into the calorimeter. A typical titration involved 25 injections (10 injection in case of compound **10**) of ligand (10 μL aliquots per shot), at 3 min intervals, into the sample cell (volume 1.4359 mL) containing tubulin. The titration cell was kept at a definite temperature and stirred continuously at 310 rpm. The data were then analyzed to determine the binding stoichiometry (N), affinity constant (K_a), and thermodynamic parameters of the reaction, using Origin 5.0 software.

Cell Culture and Maintenance. Human lung epithelium adenocarcinoma cells (A549) and human cervical carcinoma cells (HeLa) were maintained in DMEM medium supplemented with 1 mM L-glutamine, 10% fetal bovine serum, 50 μg/mL penicillin, 50 μg/mL streptomycin, and 2.5 μg/mL amphotericin B. Cells were cultured at 37 °C in a humidified atmosphere containing 5% CO_2. Cells were grown in tissue culture flasks until they were 80% confluent before trypsinisation with 1× trypsin and splitting. The morphology of control and treated cells was observed by Olympus inverted microscope model CKX41.

Cell Proliferation Inhibition Assay (MTT Assay). Viability of the A549 and HeLa cells, in the presence of varying concentrations of curcumin and compound **7** were assessed by MTT assay. Cultured A549 and HeLa cells were grown in 96-well culture plates (1×10^4 cells per well), treated with different concentrations of curcumin (0−50 μM) and compound **7** (0−50 μM), and incubated for 48 h. After incubation, 50 μL of MTT (2 mg/mL) solution in PBS were added to each well. This was incubated until a purple precipitate was visible. The absorbance was measured on an ELISA reader (MultiskanEX, Lab systems, Helsinki, Finland) at a test wavelength of 570 nm and a reference wavelength of 650 nm.

Cell Cycle Analysis by Flow Cytometry. HeLa cells (1×10^6 cells/ml) were treated without and with 2 μM nocodazole for 20 h. Nocodazole was washed off, and fresh medium containing 5 μM curcumin and 5 μM compound **7** was added. The untreated and treated cells were incubated for 8 h, fixed in ice chilled methanol for at least 30 min in 4 °C, and incubated for 4 h at 37 °C in a PBS solution containing 1 mg/mL RNase A. The nuclear DNA was then labeled with propidium iodide (PI). Cell cycle analysis was performed using the Becton Dickinson FACS Caliber, and the data were analyzed using Cell Quest program from Becton Dickinson.

Analysis for Apoptosis by Flow Cytometry. Apoptosis was measured using flow cytometry by annexin V (1 μg/mL) and PI (0.5 μg/mL) double staining. Around 1×10^6 A549 and HeLa cells were treated with curcumin (0−5 μM) and compound **7** (0−5 μM), respectively, and incubated for 48 h. Cells were then stained for 15 min at room temperature in the dark with fluorescein isothiocyanate (FITC)-conjugated annexin V (1 μg/mL) and PI (0.5 μg/mL) in a Ca^{2+}-enriched binding buffer. Annexin V-FITC and PI emissions were detected in the FL1 and FL2 channels of a FACS Caliber flow cytometer, using emission filters of 525 and 575 nm, respectively. For each sample, 10000 cells were counted. Apoptosis analysis was performed using the Becton Dickinson FACS Caliber. The data were analyzed using Cell Quest program from Becton Dickinson.

Sample Preparation for Confocal Microscopy. Cultured A549 and HeLa cells were grown at a density of 10^6 cells/mL and incubated in the presence of curcumin (0−2.5 μM) and compound **7** (0−2.5 μM), respectively, for 24 h. Subsequently cells were washed twice by PBS, fixed with 2% *para*-formaldehyde, and incubated with permeable solution (0.1% Na citrate, 0.1% Triton) for 1 h. Cells were then mildly washed with PBS, and the nonspecific binding sites were blocked by incubating the cells with 5% BSA. Subsequently, cells were incubated with antimouse monoclonal anti-α-tubulin antibody (1:200 dilutions, Sigma, USA), followed by anti mouse rhodamine conjugated IgG antibody (1:150 dilutions, GeNei, India) and DAPI (1 μg/mL). After incubation, cells were washed with PBS and viewed under a Ziess LSM 510 Meta confocal microscope.

Fluoresence Resonance Energy Transfer (FRET). The efficiency (E) of FRET between curcumin and colchicine, both tubulin-bound, was estimated from curcumin fluorescence quenching studies in presence of tubulin (λ_{ex} = 350 nm; λ_{em} = 427 nm; PEM buffer pH 7.0; 30 °C). Fluorescence intensities of 5 μM colchicine, in absence (F_o), and in presence of 10 μM of curcumin (F), yielded $E = 1 - F/F_o$. The distance (r) between tubulin-bound colchicine and curcumin was subsequently estimated from the relationship: $E = (R_o^6)/(R_o^6 + r^6)$, where R_o is the Forster distance between the donor (colchicine) and the acceptor (curcumin). R_o (in Å) was estimated using the following relationship:

$$R_o = 9.78 \times 10^3 \left[\kappa^2 n^{-4} Q_D \left(\int F_D(\lambda)\varepsilon_A(\lambda)\lambda^4 \, d\lambda\right)\right]^{1/6}$$

where κ^2 is the orientation factor, n is the refractive index of the medium, Q_D is the fluorescence quantum yield of the donor in absence of the acceptor, $F_D(\lambda)$ is the corrected (and normalized) fluorescence intensity of the donor, and $\varepsilon_A(\lambda)$ is the molar extinction coefficient of the acceptor.

Molecular Modeling Study. The crystal structure tubulin complexed with stathmin-like domain (PDB (Protein Data Bank) ID: 1SA0)[40] was used to obtain the model structure. The energy minimized atomic coordinates of compound **7** was generated using Corina (http://www.molecular-networks.com/online_demos/corina). Docking models were obtained using the PatchDock.[41] Patchdock is a geometry-based molecular docking algorithm. It divides interacting molecules surfaces into patches according to the surface shape (concave, convex, or flat). Then it applies the geometric hashing algorithm to match concave patches with convex patches and flat patches with flat patches and generates a set of candidate transformations. Each candidate transformation is further evaluated by a set of scoring functions that estimate both the shape complementarity and the atomic desolvation energy[42] of the obtained complex. Finally, redundant solutions are discarded by the application of an rmsd (root-mean-square deviation) clustering. PatchDock is highly efficient because it utilizes advanced data structures and spatial pattern detection techniques which are based on matching of local patches. The local shape information is then extended and integrated to achieve global solutions. The algorithm implicitly addresses surface flexibility by allowing minor penetrations. The best solution was retained for further analysis. The solution obtained using Patch Dock was further verified using other docking programs like GOLD[43] and Auto Dock (http://autodock.scripps.edu/resources). PyMol (http://www.pymol.org) was used for visualization and for the identification of residues in the binding pocket (within a distance of 4.5 Å of the drug).

■ ASSOCIATED CONTENT

Supporting Information. Additional experimental details; effect of different curcumin analogue on tubulin polymerization; comparative effect of curcumin and compound **7** stimulated mitotic delay on nocodazole treated HeLa cells; nuclear aberration in A549 cells by compound **7**; effect of curcumin and compound **7** on cellular morphology of HeLa and A549 cells; chemical structure of colchicines and AC colchicines; compound **2** binding on tubulin−AC complex; ^{1}H NMR, ^{13}C NMR, MS, and HPLC spectra of single ring curcumin analogue. This material is available free of charge via the Internet at http://pubs.acs.org.

AUTHOR INFORMATION

Corresponding Authors

*For B.B.: phone, 91-33-2337-9544; E-mail: bablu@boseinst.ernet.in. For A.S.: phone, 91-11- 26717121; E-mail, surolia@nii.res.in.

ACKNOWLEDGMENT

This work is supported in part by grant from the Department of Atomic Energy (DAE) to B. Bhattacharyya as a Raja Ramanna fellow.

ABBREVIATIONS USED

PIPES, piperazine-*N*,*N*′-bis(2-ethanesulphonic acid); EGTA, ethylene glycol-bis(β-aminoethyl ether)*N*,*N*,*N*′,*N*′-tetraacetic acid; $MgCl_2$, magnesium chloride; GTP, guanosine-5′-triphosphate; PDB, Protein Data Bank; ITC, isothermal titration calorimetry; AC, [2-methoxy-5-(2′,3′,4′-trimethoxyphenyl)tropone]; SAR, structure−activity relationship; FRET, fluorescence resonance energy transfer

REFERENCES

(1) Correia, J. J.; Lobert, S. Physiochemical aspects of tubulin-interacting antimitotic drugs. *Curr. Pharm. Des.* **2001**, *7*, 1213–1228.

(2) Jordan, A.; Hadfield, J. A.; Lawrence, N. J.; McGown., A. T. Tubulin as a target for anticancer drugs: agents which interact with the mitotic spindle. *Med. Res. Rev.* **1998**, *18*, 259–296.

(3) Chen, G. K.; Durán, G. E.; Mangili, A.; Beketic-Oreskovic, L.; Sikic, B. I. MDR1 activation is the predominant resistance mechanism selected by vinblastine in MES-SA cells. *Br. J. Cancer* **2000**, *83*, 892–896.

(4) Orr, G. A.; Verdier-Pinard, P.; McDaid, H.; Horwitz, S. B. Mechanisms of taxol resistance related to microtubules. *Oncogene* **2003**, *22*, 7280–7295.

(5) Pannacciulli, I.; Ballarino, P.; Castello, G.; Arboscello, E.; Botta, M.; Tredici, S.; Lerza., R. In vitro toxicity of taxol based anticancer drug combinations on human hemopoietic progenitors. *Anticancer Res.* **1999**, *19*, 409–412.

(6) Sun, W.; Wang, W.; Kim, J.; Keng, P.; Yang, S.; Zhang, H.; Liu, C.; Okunieff, P.; Zhang, L. Anti-cancer effect of resveratrol is associated with induction of apoptosis via a mitochondrial pathway alignment. *Adv. Exp. Med. Biol.* **2008**, *614*, 179–186.

(7) Mukherjee, S.; Acharya, B. R.; Bhattacharyya, B.; Chakrabarti, G. Genistein arrests cell cycle progression of A549 cells at the G_2/M phase and depolymerizes interphase microtubules through binding to a unique site of tubulin. *Biochemistry* **2010**, *49*, 1702–1712.

(8) Sarkar, F. H.; Li, Y. Harnessing the fruits of nature for the development of multitargeted cancer therapeutics. *Cancer Treat. Rev.* **2009**, *35*, 597–607.

(9) Dhillon, N.; Aggarwal, B. B.; Newman, R. A.; Wolff, R. A.; Kunnumakkara, A. B.; Abbruzzese, J. L.; Ng, C. S.; Badmaev, V.; Kurzrock, R. Phase II trial of curcumin in patients with advanced pancreatic cancer. *Clin. Cancer. Res.* **2008**, *14*, 4491–4499.

(10) Aggarwal, B. B.; Sung, B. Pharmacological basis for the role of curcumin in chronic diseases: an age-old spice with modern targets. *Trends Pharmacol. Sci.* **2009**, *30*, 85–94.

(11) Goel, A.; Kunnumakkara, A. B.; Aggarwal, B. B. Curcumin as "Curecumin": from kitchen to clinic. *Biochem. Pharmacol.* **2008**, *75*, 787–809.

(12) Kawamori, T.; Lubet, R.; Steele, V. E.; Kelloff, G. J.; Kaskey, R. B.; Rao, C. V.; Reddy, B. S. Chemopreventive effect of curcumin, a naturally occurring antiinflammatory agent, during the promotion/progression stages of colon cancer. *Cancer. Res.* **1999**, *59*, 597–601.

(13) Mackenzie, G. G.; Queisser, N.; Wolfson, M. L.; Fraga, C. G.; Adamo, A. M.; Oteiza, P. I. Curcumin induces cell-arrest and apoptosis in association with the inhibition of constitutively active NF-kappaB and STAT3 pathways in Hodgkin's lymphoma cells. *Int. J. Cancer* **2008**, *123*, 56–65.

(14) Van Erk, M. J.; Teuling, E.; Staal, Y. C.; Huybers, S.; Van Bladeren, P. J.; Aarts, J. M.; Van Ommen, B. Time- and dose-dependent effects of curcumin on gene expression in human colon cancer cells. *J Carcinog.* **2004**, *3*, 8.

(15) Jana, N. R.; Dikshit, P.; Goswami, A.; Nukina, N. Inhibition of proteasomal function by curcumin induces apoptosis through mitochondrial pathway. *J. Biol. Chem.* **2004**, *279*, 11680–11685.

(16) Anto, R. J.; Mukhopadhyay, A.; Denning, K.; Aggarwal, B. B. Curcumin (diferuloylmethane) induces apoptosis through activation of caspase-8, BID cleavage and cytochrome c release: its suppression by ectopic expression of Bcl-2 and Bcl-xl. *Carcinogenesis* **2002**, *23*, 143–150.

(17) Aggarwal, B. B.; Kumar, A.; Bharti, A. C. Anticancer potential of curcumin: preclinical and clinical studies. *Anticancer Res.* **2003**, *23*, 363–298.

(18) Qiu, X.; Du, Y.; Lou, B.; Zuo, Y.; Shao, W.; Huo, Y.; Huang, J.; Yu, Y.; Zhou, B.; Du, J.; Fu, H.; Bu, X. Synthesis and identification of new 4-arylidene curcumin analogs as potential anticancer agents targeting nuclear factor-κB signaling pathway. *J. Med. Chem.* **2010**, *53*, 8260–8273.

(19) Gupta, K. K.; Bharne, S. S.; Rathinasamy, K.; Naik, N. R.; Panda, D. Dietary antioxidant curcumin inhibits microtubule assembly through tubulin binding. *FEBS J.* **2006**, *273*, 5320–5332.

(20) Banerjee, M.; Singh, P.; Panda, D. Curcumin suppresses the dynamic instability of microtubules, activates the mitotic checkpoint and induces apoptosis in MCF-7 cells. *FEBS J.* **2010**, *277*, 3437–3448.

(21) Fourest-Lieuvin, A.; Peris, L.; Gache, V.; Garcia-Saez, I.; Juillan-Binard, C.; Lantez, V.; Job, D. Microtubule regulation in mitosis: tubulin phosphorylation by the cyclin-dependent kinase Cdk1. *Mol. Biol. Cell* **2006**, *17*, 1041–1050.

(22) Hearn, B. R.; Shaw, S. J.; Myles, D. C. Microtubule targeting agents. *Compr. Med. Chem. II* **2007**, *7*, 81–110.

(23) RayChaudhuri, A.; Tomita, I.; Mizuhashi, F.; Murata, K.; Ludueña, R. F. Distinct and overlapping binding sites for IKP104 and vinblastine on tubulin. *J. Protein Chem.* **1998**, *17*, 685–690.

(24) Wang, Y. J.; Pan, M. H.; Cheng, A. L.; Lin, L. I.; Ho, Y. S.; Hsieh, C. Y.; Lin, J. K. Stability of curcumin in buffer solutions and characterization of its degradation products. *J. Pharm. Biomed. Anal.* **1997**, *12*, 1867–1876.

(25) Mishra, S.; Karmodiya, K.; Surolia, N.; Surolia, A. Synthesis and exploration of novel curcumin analog as antimalarial agents. *Bioorg. Med. Chem.* **2008**, *16*, 2894–2902.

(26) Schön, A.; Madani, N.; Smith, A. B.; Lalonde, J. M.; Freire, E. Some binding-related drug properties are dependent on thermodynamic signature. *Chem. Biol. Drug Des.* **2011**, *77*, 161–165.

(27) Perozzo, R.; Folkers, G.; Scapozza, L. Thermodynamics of protein−ligand interactions: history, presence, and future aspects. *J. Recept. Signal Transduction Res.* **2004**, *24*, 1–52.

(28) Kauzmann, W. Some factors in the interpretation of protein denaturation. *Adv. Protein Chem.* **1959**, *14*, 1–63.

(29) Baldwin, R. L. Temperature dependence of the hydrophobic interaction in protein folding. *Proc. Natl. Acad. Sci. U.S.A.* **1986**, *83*, 8069–8072.

(30) Freire, E. Do enthalpy and entropy distinguish first in class from best in class? *Drug Discovery Today* **2008**, *13*, 869–874

(31) Eisinger, J. Intermolecular energy transfer in adrenocorticotropin. *Biochemistry* **1969**, *8*, 3902–3908.

(32) Löwe, J.; Li, H.; Downing, K. H.; Nogales, E. Refined structure of alpha beta-tubulin at 3.5 Å resolution. *J. Mol. Biol.* **2001**, *313*, 1045–1057.

(33) Dorléans, A.; Gigant, B.; Ravelli, R. B.; Mailliet, P.; Mikol, V.; Knossow, M. Variations in the colchicine-binding domain provide insight into the structural switch of tubulin. *Proc. Natl. Acad. Sci. U.S.A.* **2009**, *106*, 13775–13779.

(34) Jackman, R. W.; Rhoads, M. G.; Cornwell, E.; Kandarian, S. C. Microtubule-mediated NF-kappaB activation in the TNF-alpha signaling pathway. *Exp. Cell. Res.* **2009**, *315*, 3242–3249.

(35) Mackenzie, G. G.; Keen, C. L.; Oteiza, P. I. Microtubules are required for NF-kappaB nuclear translocation in neuroblastoma IMR-32 cells: modulation by zinc. *J. Neurochem.* **2006**, *99*, 402–415.

(36) Chiriac, I. C.; Tanasa, F.; Onciu, M. A Novel approach in cinnamic acid synthesis: direct synthesis of cinnamic acids from aromatic aldehydes and aliphatic carboxylic acids in the presence of boron tribromide. *Molecules* **2005**, *10*, 481–487.

(37) Lin, C. M.; Hamel, E. Effects of inhibitors of tubulin polymerization on GTP hydrolysis. *J. Biol. Chem.* **1981**, *256*, 9242–9245.

(38) Banerjee, A.; Luduena, R. F. Kinetics of association and dissociation of colchicine−tubulin complex from brain and renal tubulin. Evidence for the existence of multiple isotypes of tubulin in brain with differential affinity to colchicine. *FEBS Lett.* **1987**, *219*, 103–107.

(39) Abou-Zied, O. K.; Al-Shihi, O. I. Characterization of subdomain IIA binding site of human serum albumin in its native, unfolded, and refolded states using small molecular probes. *J. Am. Chem. Soc.* **2008**, *130*, 10793–10801.

(40) Ravelli, R. B.; Gigant, B.; Curmi, P. A.; Jourdain, I.; Lachkar, S.; Sobel, A.; Knossow, M. Insight into tubulin regulation from a complex with colchicine and a stathmin-like domain. *Nature* **2004**, *428*, 198–202.

(41) Schneidman-Duhovny, D.; Inbar, Y.; Nussinov, R.; Wolfson, H. J. PatchDock and SymmDock: servers for rigid and symmetric docking. *Nucl. Acids. Res.* **2005**, *33*, 363–367.

(42) Benyamini, H.; Shulman-Peleg, A.; Wolfson, H. J.; Belgorodsky, B.; Fadeev, L.; Gozin, M. Interaction of C(60)-fullerene and carboxyfullerene with proteins: docking and binding site alignment. *Bioconjugate Chem.* **2006**, *17*, 378–386.

(43) Jones, G.; Willett, P.; Glen, R. C.; Leach, A. R.; Taylor, R. Development and validation of a genetic algorithm for flexible docking. *J. Mol. Biol.* **1997**, *267*, 727–748.